
U-SPECT-I: A Novel System for Submillimeter-Resolution Tomography with Radiolabeled Molecules in Mice

Freek J. Beekman, PhD^{1,2}; Frans van der Have, MSc^{1,2}; Brendan Vastenhouw, MSc^{1,2}; Annemarie J.A. van der Linden, BSc²; Peter P. van Rijk, MD, PhD¹; J. Peter H. Burbach, PhD²; and Marten P. Smidt, PhD²

¹Department of Nuclear Medicine, Image Sciences Institute, University Medical Center Utrecht, Utrecht, The Netherlands; and
²Department of Pharmacology and Anatomy, University Medical Center Utrecht, Utrecht, The Netherlands

A major advance in biomedical science and diagnosis was accomplished with the development of *in vivo* techniques to image radiolabeled molecules, but limited spatial resolution has slowed down applications to small experimental animals. Here, we present a SPECT system (U-SPECT-I) dedicated to radionuclide imaging of murine organs at a submillimeter resolution.

Methods: The high performance of U-SPECT-I is based on a static triangular detector setup, with a cylindrical imaging cavity in the center and 75 gold micropinhole apertures in the cavity wall. The pinholes are focused on a small volume of interest such as the mouse heart or spine to maximize the detection yield of γ -photons. Three-dimensional molecular distributions are iteratively estimated using the detector data and a statistical reconstruction algorithm that takes into account system blurring and data noise to increase resolution and reduce image noise. **Results:** With 0.6-mm-diameter pinholes, the maximum fraction of detected photons emitted by a point source (peak sensitivity) is 0.22% for a 15%-wide energy window and remains higher than 0.12% in the central 12 mm of the central plane. In a resolution phantom, radioactively filled capillaries as small as 0.5 mm and separated by 0.5 mm can be distinguished clearly in reconstructions. Projection data needed for the reconstruction of cross sections of molecular distributions in mouse organs can readily be obtained without the need for any mechanical movements. Images of a mouse spine show ^{99m}Tc-hydroxymethylene diphosphonate uptake down to the level of tiny parts of vertebral processes. These are separated clearly from the vertebral and intervertebral foramina. Using another tracer, one can monitor myocardial perfusion in the left and right ventricular walls, even in structures as small as the papillary muscles. **Conclusion:** U-SPECT-I allows discrimination between molecular concentrations in adjacent volumes of as small as about 0.1 μ L, which is significantly smaller than can be imaged by any existing SPECT or PET system. Our initial *in vivo* images of the mouse heart and spine show that U-SPECT-I can be used for novel applications in the study of dynamic biologic systems with a clear projection to clinical applications. The combination of high

resolution and detection efficiency of U-SPECT-I opens up new possibilities for the suborgan-level study of radiotracers in mouse models.

Key Words: molecular imaging; pinhole; SPECT; mouse; reconstruction

J Nucl Med 2005; 46:1194–1200

Dedicated SPECT and PET instruments (*1*) in concert with the radiolabeling of small molecules, antibodies, peptides, and probes for gene expression have facilitated *in vivo* assessment of molecular mechanisms and the development of new tracers and pharmaceuticals (*2–6*). Recent developments in this multidisciplinary field of molecular imaging have initiated a revolution in biomedical sciences. A bottleneck in the assessment of molecular mechanisms at the suborgan scale is the limited spatial resolution of available SPECT and PET instruments. In practice, the resolution in living animals is presently limited to tissue volumes of about 1 μ L (e.g., (*7*)) but is often an order of magnitude larger. The increasing availability of genetically modified mice as models for human disease prompts studies with SPECT and PET. However, improving image resolution and dynamic capabilities is essential to fully exploit the disease models and tracers available.

SPECT systems using pinhole apertures permit radiolabeled molecular distributions to be imaged *in vivo* in small animals. Several pinhole-SPECT systems have been designed and constructed in recent years (*8–14*). In addition to SPECT systems, dedicated small-animal PET systems have been devised for the imaging of radiolabeled molecules (*15*). The applications of SPECT and PET partly overlap and often are complementary. The method used for a particular application depends on factors such as equipment costs, infrastructure, required resolution, and counting sensitivity and also is influenced by logistics, costs, and the availability of the specific radiomolecules required.

Received Jan. 14, 2005; revision accepted Mar. 21, 2005.

For correspondence or reprints contact: Freek J. Beekman, PhD, Department of Nuclear Medicine, Image Sciences Institute, Rudolf Magnus Institute of Neuroscience, University Medical Center Utrecht, Room STR 5.203, Universiteitsweg 100, 3584 CG, The Netherlands.

E-mail: f.beekman@azu.nl

With micropinhole radionuclide imaging, it becomes possible to obtain high-spatial-resolution projection data, particularly for small organs that can be positioned near the pinhole. For example, a study has shown that the thyroid of a living mouse (typical size, 1×1 mm) can be imaged at a resolution of as good as 0.2 mm using planar pinhole cameras (16). However, a drawback of contemporary pinhole SPECT, compared with PET, is the limited ability to detect a good fraction of the emitted γ -photons. This counting sensitivity decreases further when smaller pinholes are used to increase image resolution. With low counting sensitivity, the high-resolution information content of projection data cannot be fully exploited since reconstructed volumes calculated from these projections tend to be noisy and visual interpretation is possible only after resolution-degrading smoothing operations. These often result in a resolution that is significantly worse than that of images obtained with small-animal PET.

The goal of the present paper is the launching of a dedicated mouse SPECT system (U-SPECT-I), developed at University Medical Center Utrecht, that defines a new front line of small-animal SPECT characteristics through a design that enables one to exploit the high-resolution content of pinhole projection data. U-SPECT-I is stationary in the sense that there is no need for moving any of the parts, such as the detector and the collimator, or the animal. The resultant advantages include system stability, simplicity of system design, the flexibility of performing dynamic studies with any frame-time (14,17,18), and ease of animal handling and positioning. In addition, U-SPECT-I is designed such that all pinholes focus on a small area. In this way, a specific object area is adequately magnified on the detector plane, whereas only a limited part of the detector surface available is required for creating each mini camera. The use

of all these independent mini cameras together results in a significantly higher sensitivity, thus overcoming a fundamental problem of micropinhole imaging. The system is based on conventional scintillation γ -cameras that are part of a clinical SPECT system (Prism 3000 S; Picker Medical Systems) and has the flexibility to be switched back rapidly to the original clinical imaging setup. Validation of the system design and its outstanding imaging characteristics is demonstrated through imaging of specific phantoms and mouse organs.

MATERIALS AND METHODS

In this section, we describe the U-SPECT-I system geometry (composition and positioning of pinholes and detectors), the image reconstruction methods, the physical phantom experiments, and the animal experiments that proved the system performance.

Pinhole Design and Geometry of U-SPECT-I

Figure 1A shows an overview of the U-SPECT-I system, in which the detectors of a triple-head SPECT system (with clinical collimators removed) are used as a detector ring. A cylinder with 75 gold pinholes is placed in the center (Figs. 1B and 1C). The pinhole apertures are placed in a 5-fold ring geometry, with each ring containing 15 pinhole apertures. Compared with commonly used lead or tungsten, the gold pinhole apertures have high-photon-stopping power, thus reducing blurring caused by radiation penetration and scattering in the aperture edge material (19). In contrast to the earlier-proposed depleted uranium, which has an even better stopping power, gold pinholes can be manufactured quite easily in high quantities and are not radioactive or poisonous. The high-photon-counting sensitivity obtained with the large number of pinholes can be traded for increased image resolution by the use of relatively small pinholes (0.6-mm diameter). The pinholes have knife edges and an opening angle of 30° , with shielding placed in such a way that projections do not overlap (Fig. 2A). The

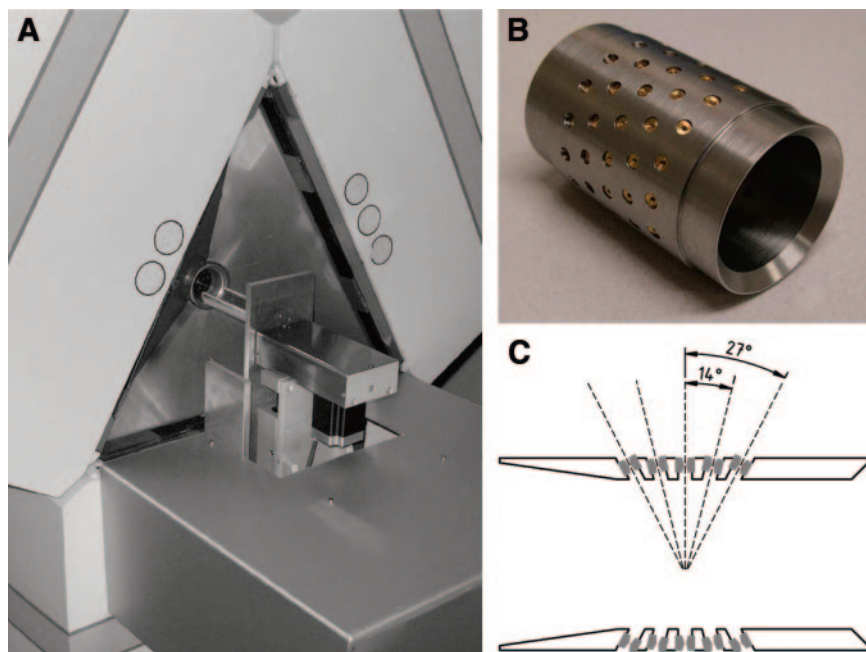


FIGURE 1. (A) Overview of U-SPECT-I system. Triangular lead shielding is placed between camera heads of triple-detector system, tungsten cylinder containing pinholes being centered within the 3 detectors. x,y,z stage with attached bed, placed in front of lower detector, is also visible. (B) Cylinder with 75 gold pinhole apertures that are focused on its center. (C) Cross section of cylinder with tilted pinholes.

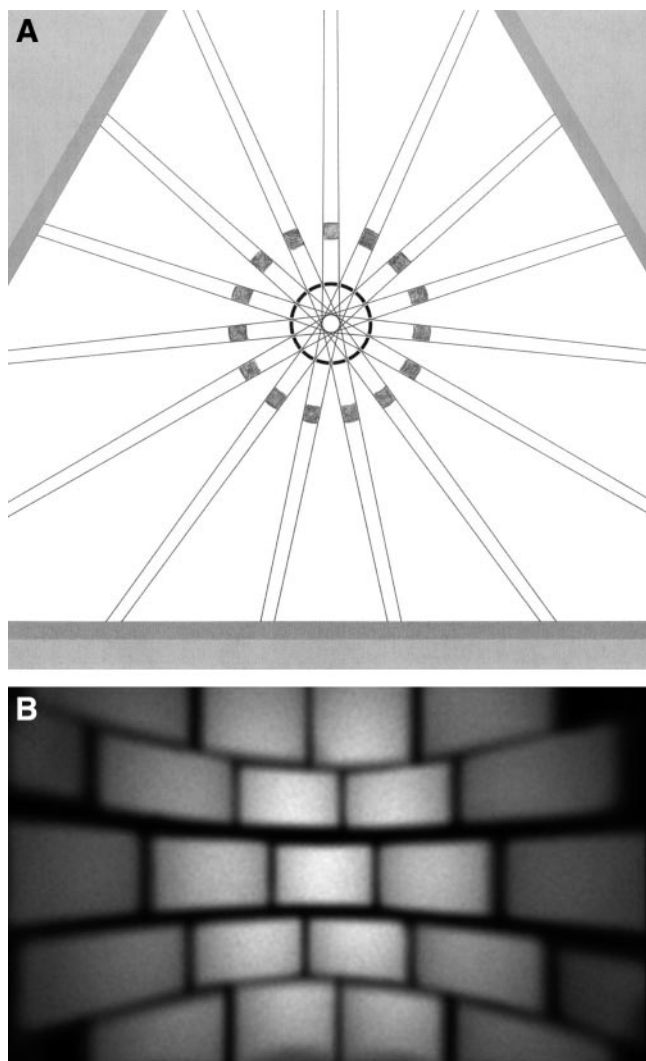


FIGURE 2. Illustration of highly focusing pinhole geometry of U-SPECT-I. (A) Cross section through 1 of 5 rings with pinholes. Lines emerging from central circle mark triangular cross sections of beams in which emitted γ -quanta can travel from animal toward detector. Pinholes in all rings focus on center to maximize detection yield. Lead cylinder with square holes shown in gray is placed around tungsten cylinder with pinholes to prevent projection overlap. (B) Radiation intensity on 1 of 3 detectors when a bottle with a ^{99m}Tc solution is imaged. Image demonstrates how the large detector is divided into a large number of small subcameras.

shielding consists of a lead tube with square holes defining the edges of the projections (Fig. 2B).

A cross section through the detector and the central ring with pinholes is shown in Figure 2A. The edges of the 15 photon beams passing through the 15 pinholes in this ring are indicated by lines that diverge from the individual pinholes toward the detector and toward the center of the cylinder. All pinholes in the various rings focus on the center. The apertures in the outer rings are placed at a wider angle to the transaxial axis. In this way, voxels in the central field of view can be observed via 69 pinholes simultaneously (6 of the 75 pinhole cameras are partly or completely blind because of a missing area of active crystal close to the camera

edges in the corners of the triangle). The pinhole positions in adjacent rings are rotated over 8° to increase the variety of angles at which each voxel is observed. The projections of the object area observed by different pinholes do not overlap. Overlap is prevented by placing a lead tube with 75 rectangular holes around the tungsten pinhole cylinder. The diameter of the rings with pinholes is 44 mm when measured at the centers of the pinhole openings. The intrinsic resolution of the γ -cameras was determined to be 3.2 mm in full width at half maximum as measured with a line-shaped beam (140 keV).

Image Reconstruction and Calibration

U-SPECT-I images were reconstructed using 150-iteration maximum-likelihood expectation maximization (20). Point spread functions (PSFs) of the system were used during maximum-likelihood expectation maximization to model the probability that a photon from a certain object position will be detected by a specific detector pixel. PSFs were measured using a 60-MBq point source. The point source was produced from a chromatographic bead, which was approximately 1 voxel. Small amounts (10–15 μL) of concentrated (approximately 4 GBq/mL) pertechnetate were added 10–15 times, and the liquid was evaporated by being heated to about 60°C . The point source was attached to its holder by a fast-curing epoxy resin.

Each PSF is part of the transition matrix, which is stored entirely on disk. Because one considers entire PSFs during reconstruction, instead of assuming a line integral through the center of each pinhole, the effects of blurring due to pinhole diameter and pinhole penetration and of blurring intrinsic to the detector are corrected for during reconstruction. Other advantages of direct measurement of PSFs are that it obviates separate calibration of mechanical (detector and collimator) and electronics offsets and correction of uniformity and linearity.

The measured PSFs over all voxels in the cylinder together represent the entire system matrix needed during iterative reconstruction of the image. A similar method has been used to calibrate the FASTSPECT system of the University of Arizona (18). With the U-SPECT-I system, the voxel size used in reconstructions is small (0.1875 mm). The projection pixel size used for all measurements reported in this paper was 0.898 mm. Because it would be time consuming to separately measure the PSF for each voxel position in the pinhole cylinder, we measured the PSF in a subset of voxels in the object using an x,y,z stage and a grid of $7 \times 7 \times 11$ points with a spacing of 3 mm, 3 mm, and 1.5 mm, respectively. For each measured PSF, we first estimated 3 basic properties: the coordinates of the maximum on the detector, the flux, and the width. Using linear interpolation and extrapolation, we estimated and stored the properties of the missing PSFs.

Study of System Characteristics

Position-dependent point-source sensitivity in the collimator ring was measured using the same scanning point source as used for system calibration. The sensitivity profiles presented in Figure 3 were acquired over 3 mutually perpendicular axes, each crossing the center of the field of view, and were obtained with a 15% energy window.

A miniature acrylic resolution phantom (Derenzo phantom) was manufactured. It contained 6 sectors, each containing equally sized sets of capillaries (0.4, 0.5, 0.6, 0.7, 0.8, and 1.0 mm). Each capillary was 10 mm long, the total activity in all capillaries together was 11.1 MBq of ^{99m}Tc , and the data acquisition time was 30 min. The distance between the rods equaled the rod diameter.

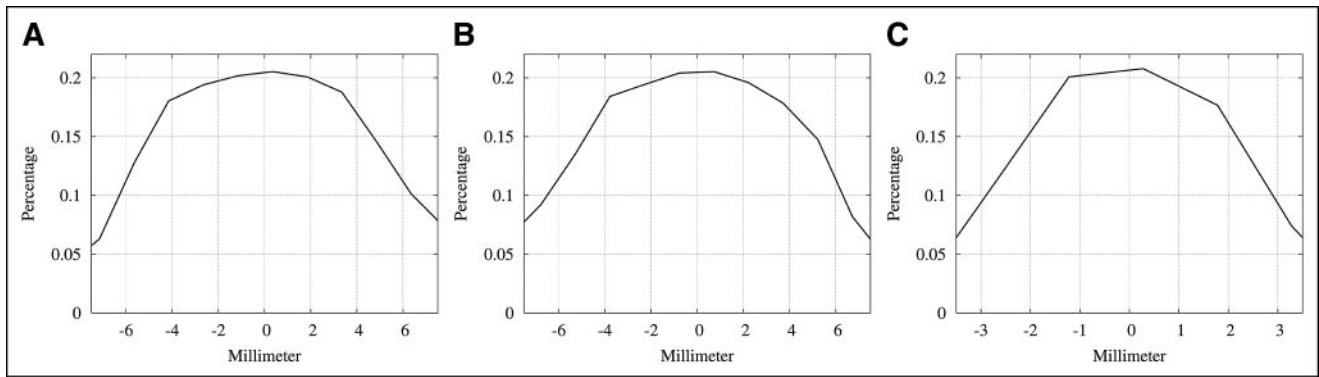


FIGURE 3. Demonstration of high sensitivity of U-SPECT-I. Shown are sensitivity profiles lying along mutually orthogonal lines that cross the center of field of view, obtained with a scanning point source: along *x*-axis (A), along *y*-axis (B), and along transaxial axis (*z*-axis) (C).

The phantom diameter was 12 mm. The spatial resolution in such phantoms is often defined by the size of capillaries that can be observed separately.

Animal Studies

Animal studies were conducted following protocols approved by the Animal Research Committee of the University Medical Center Utrecht. Three-month-old C57BL/6JO1aHsd mice (body weight, 25–30 g; Harlan) were anesthetized with a mix of 2.5 mL of Hypnorm (fentanyl, 0.315 mg/mL, and fluanisone, 10 mg/mL; Janssen), 2.5 mL of Dormicum (midazolam, 5 mg/mL; Roche), and 5 mL of Aquadest, administered intraperitoneally, per kilogram of body weight. Thereafter, the radionuclide of interest (0.2-mL solution) was injected into the tail vein. The radionuclides tested were ^{99m}Tc -hydroxymethylene diphosphonate (HDP) for bone imaging and ^{99m}Tc -tetrofosmin for cardiac perfusion imaging. During the entire procedure, animal body temperature was kept at 37°C.

RESULTS

Ultrahigh System Sensitivity and Image Resolution

Sensitivity, here expressed as the percentage of emitted γ -quanta that are detected, depends on the pinhole diameter, the number of pinholes, and the distance of the pinholes to the object (21,22). The peak sensitivity with 0.6-mm pinholes was measured to be 0.22% in the central field of view and remained 0.12% within a central transaxial disk with a 12-mm diameter (Fig. 3). Sensitivities of other small-animal SPECT systems are typically more than an order of magnitude lower when compared at equal geometric system resolution, because of a low number of pinholes or the less-focusing architecture. High sensitivity is crucial to avoid noisy data and therefore to avoid excessive resolution-degrading low-pass filtering for enhancing the appearance of otherwise-noisy reconstructed images. For any pinhole system, the sensitivity can be increased at the cost of system resolution, by enlarging the pinholes.

Imaging of the miniature resolution phantom during 30 min resulted in reconstructions clearly resolving the set of 0.5-mm capillaries (Fig. 4). Even some of the 0.4-mm capillaries could be identified. This result indicates that

differences in molecular uptake between tiny neighboring tissue volumes on the order of 0.1 μL can readily be distinguished. Note that the smallest capillaries resolved with state-of-the-art PET scanners are approximately 1 mm (7) when advanced statistical reconstruction is applied.

Ultra-High-Resolution Images of Radiomolecules in Live Mice

To show that highly detailed imaging can be extrapolated from test objects to live animals, we acquired images of mice with 2 different tracers often used in clinical SPECT studies. Figure 5 shows 3 perpendicular cross sections of a myocardial perfusion volume image obtained with ^{99m}Tc -tetrofosmin. Myocardial perfusion in both the left and the right ventricular walls is clearly visible. Perfusion in the anterior papillary muscle within the left ventricle was readily distinguished in the short-axis slice (arrow). The level of detail presented here may lead to new experimental opportunities in cardiology.

A second experiment was performed to show bone metabolism within a mouse lumbar spine (Fig. 6). Three 0.25-mm-thick orthogonal slices through the spine are presented.

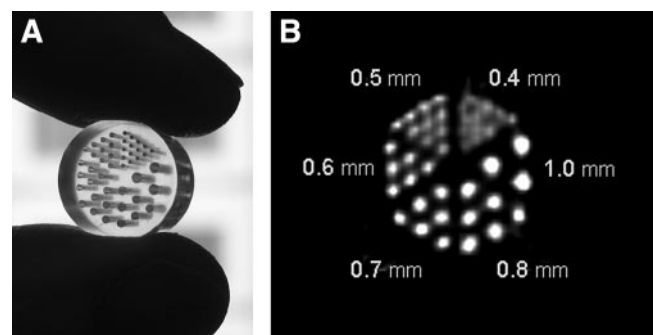


FIGURE 4. Demonstration of submillimeter resolution of U-SPECT-I images. (A) Photograph of miniature acrylic resolution phantom with capillaries used as test object. (B) Reconstructed cross-sectional image, with a slice thickness of 0.5 mm, of the phantom shown in A. Half-millimeter capillaries are clearly separated on image.

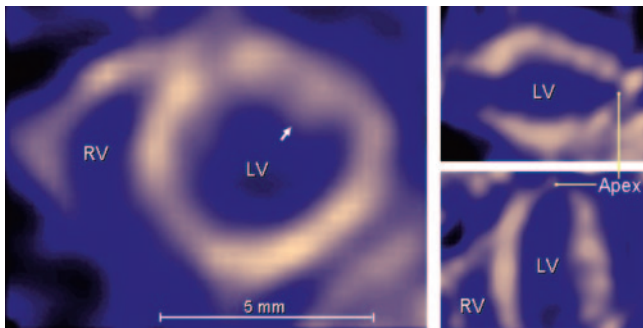


FIGURE 5. Mutual perpendicular cross sections through submillimeter-resolution 3-dimensional myocardial perfusion image volume of living mouse (named Animal Co-Image of the Year at the annual meeting of the Society of Nuclear Medicine, Philadelphia, 2004). Image data were acquired during 30 min, starting 30 min after administration of 222 MBq (6 mCi) of ^{99m}Tc -tetrafosmin. On left is a short-axis slice showing myocardial perfusion in right ventricular (RV) and left ventricular (LV) walls. Perfusion in anterior papillary muscle (arrow) can be distinguished from other parts of left ventricular wall. At top right is a vertical long-axis slice; at bottom right, a horizontal long-axis slice.

A projection of local image maxima (maximum-intensity projection) and isosurface renderings were calculated from the same reconstructed 3-dimensional tracer distribution. ^{99m}Tc -HDP uptake in tiny parts of the individual processes and other tiny vertebral parts was readily visualized. Also, the spaces between and within the vertebrae, intervertebral foramen, and vertebral foramen that do not take up ^{99m}Tc -HDP were clearly distinguished from bone tissue, particularly in the isosurface renderings. Because uptake of ^{99m}Tc -HDP-like agents is very much influenced by changes in bone remodeling, such as those caused by mechanical strain or tumor growth, the type of detailed imaging shown here may initiate new research opportunities in locomotion, bone, and cancer research.

DISCUSSION

In this paper, we have described a new SPECT system that has a highly focused pinhole architecture resulting in high-resolution molecular imaging. Even with standard detectors with an intrinsic resolution of 3.2 mm, SPECT images with a resolution better than 0.5 mm were obtained, without the optimizing of pinhole diameters. U-SPECT-I, and its successors with an even higher resolution, will allow the 3-dimensional assessment of distributions of a wide range of radiolabeled tracers. Labor-intensive in vitro or ex vivo methods may be replaced in several cases by the imaging of intact animals on the submillimeter level, also allowing for accurate longitudinal study designs, instrumental for development of new diagnostic or therapeutic agents. Importantly, U-SPECT-I allows noninvasive imaging of mice with radionuclides and associated radiomolecules, many of which are already approved for clinical use. On the other hand, novel imaging applications and tracer biology developed in mice can readily be applied to the clinical setting, in which radionuclide imaging methods such as SPECT are already in common use.

The present U-SPECT-I system has an outstanding sensitivity/resolution trade-off, with a field of view that is large enough to cover most essential mouse organs, such as the entire midbrain, the mouse heart, or the lumbar spine. Often only small fields of view are required. The advantage of the focusing setup is that one can acquire many photons from a specific area of interest. As we have shown, this helps to produce a high image resolution. It is possible to extend the field of view without changing the pinhole geometry: The bed has then to be shifted in order to focus the pinholes on different areas of the animal. As a result, the area with highest sensitivity is scanned through the volume of interest in the animal. The most trivial way to extend the field of view is to stitch together the smaller images calculated from

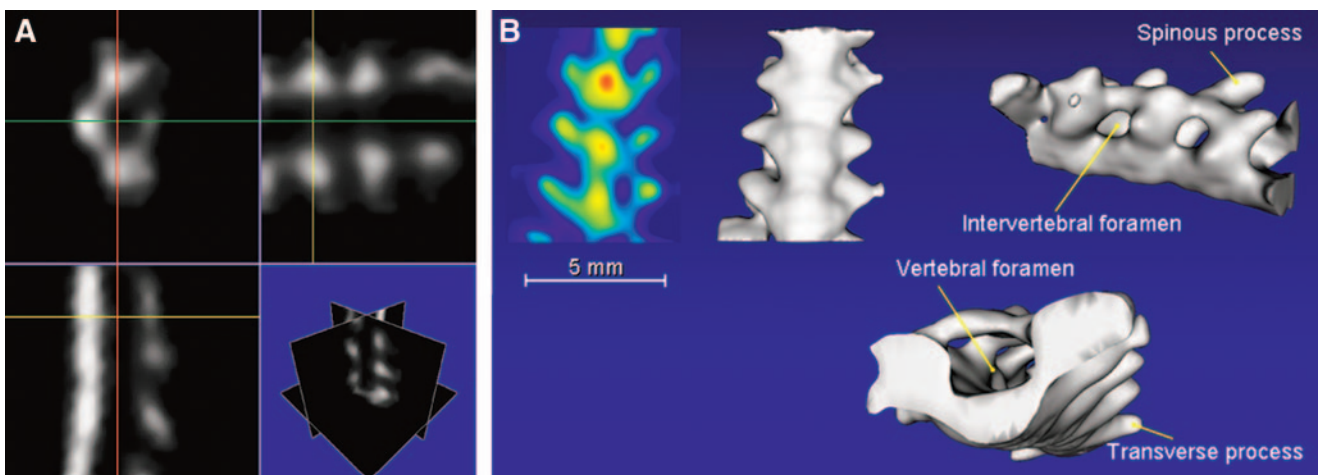


FIGURE 6. Different representations of reconstructed image volume of lumbar spine, acquired during 22 min, 2 h after injection of 148 MBq (4 mCi) of ^{99m}Tc -HDP. (A) Three different orthogonal cross sections. (B) Projection of local image maxima (far left) and 3 isosurface renderings of tracer concentrations in same spinal section (named Animal Co-Image of the Year at the annual meeting of the Society of Nuclear Medicine, Philadelphia, 2004).

separate acquisitions, as is often done in clinical procedures. However, we have devised a more promising solution that consists of a combined reconstruction and acquisition strategy that simultaneously takes into account all projection data from different bed positions and produces the entire image volume from a single reconstruction (23). With this method, it may be possible to extend the useful field of view to the entire central nervous system of a mouse by using no more than 2 bed positions. Positions can be alternated sufficiently rapidly by shifting back and forth the tiny bed instead of the heavy detectors, enabling dynamic studies with an extended field of view.

Another way to extend the field of view of the U-SPECT-I system is to remove the cylindrical shielding between the pinholes and the detector (Fig. 2A). As a result, the projections will overlap to a certain extent, the degree of which will depend on the shape of the pinholes, such as the opening angle and type of edge. Systems with overlapping projections (e.g., (12)) have another interesting feature: They can detect a larger fraction of the emitted photons while activity that is concentrated in small areas such as small tumors can still be projected on separate areas on the detector. On the other hand, for the extended distributions that are more common in biology, the overlap of patterns on the detector will lead to significant loss of information about the emission direction of each detected γ -quantum. Whether the increase in detection probability obtained by overlap will compensate for such an information loss strongly depends on the specific distribution of the molecules to be imaged, on the amount of projection overlap, and on the number of detected photons. These will be important factors determining whether the same increase of sensitivity might be better obtained by using larger pinholes instead of more pinholes combined with overlap. Comparisons of the image quality of systems with overlapping projections and with nonoverlapping projections will be a research subject of continuing interest. In addition, several novel (hybrid) projection strategies are currently being developed in our laboratory.

An important cause of the low sensitivity of previously proposed pinhole SPECT systems is that the γ -detection depends on traditional Anger scintillation cameras with a typical intrinsic resolution of approximately 2.0–4.0 mm. Higher-resolution detectors are still extremely expensive if they are required to cover a large area. The problem of limited detector resolution is bypassed with pinhole SPECT, through the application of a significant magnification of the animal via the pinhole on the detector. For adequately magnified projection of a large part of the animal, one needs a large detector surface area. This is why in almost all systems only a few pinhole cameras are placed around the animal; more pinholes would cause overlapping of the projections. With a few pinholes, the resulting bulky cameras need to be rotated to obtain projections at a sufficient number of angles. The required mechanics complicate these SPECT systems and make them difficult to calibrate. In

addition, systems requiring detector rotation have only limited flexibility in acquiring and processing dynamic series.

The design of U-SPECT-I allows for stationary acquisition of projection data, similar to the type of acquisitions possible with the FASTSPECT system (18) and PET systems. Together with the high sensitivity achieved with the high number of pinholes, U-SPECT-I will enable researchers to perform dynamic studies on mice, and users will have greater flexibility in choosing frame time a posteriori. Additionally the design, having no moving parts, will reduce maintenance and may simplify system calibration.

Previous simulation studies (14) of stationary small-animal SPECT devices have indicated that the results with higher-resolution detectors will be significantly better than those presented here, that the focused pinhole geometry with nonoverlapping projection views brings us closer to satisfying Orlov's conditions for adequate sampling of data (24) than do traditional pinhole SPECT systems, and that this is important for producing better results than are possible with traditional pinhole SPECT systems that acquire projections over a single orbit.

U-SPECT-I is based on the use of a triangular scintillation detector setup "borrowed" from a system currently in use for routine clinical SPECT. The entire transformation from U-SPECT-I back to the clinical system takes about 10 min, and no extra calibrations are required between the switching from clinical to animal imaging device. Therefore, the U-SPECT-I design is extremely cost-effective and can universally be applied to clinical SPECT systems. Ultimately, however, stationary SPECT systems may comprise a detector ring or a spheric layer (a sphere concluded by 2 planes), approximated by a polygon that is formed by high-resolution detectors, such as in the U-SPECT-III design (14). High-resolution detectors are under development by several groups (e.g., (25–29)). A next step in U-SPECT evolution will be the application of such detectors. U-SPECT-III has already been tested in simulations, but the costs and availability of detectors are restrictive. Simulation results point to marked progress in small-animal SPECT instrumentation over the next couple of years.

CONCLUSION

U-SPECT-I defines a new front line in small-animal SPECT. It is a fully functional, dedicated small-animal SPECT system with an outstanding volumetric resolution on the order of 0.1 μ L. Results indicate that resolution is significantly better with U-SPECT-I than with state-of-the-art small-animal SPECT and PET systems. The system allows for assessing tracer dynamics in suborgans of the living mouse, as was illustrated by *in vivo* images showing submillimeter details of molecular uptake in the myocardium and vertebrae. The high resolution, high sensitivity, and relatively low hardware costs of U-SPECT-I should now allow detailed molecular imaging to be applied successfully to a wide range of study types, thus creating a

broad range of new experimental opportunities. Significant improvements in image quality are expected when the triangular detector setup of U-SPECT-I is replaced by high-resolution detectors.

ACKNOWLEDGMENTS

This work was sponsored by the Medical Council of The Netherlands Organization for Scientific Research, grant 917.36.335. We thank Dr. Lars Furenlid for showing us how to make concentrated point sources and Dr. Simon Cherry for introducing Dr. Freek Beekman to the microimaging world. Gijs van der Wilt, Cees van der Linden, Henk te Biesebeek, Jan Brakkee, and Cora de Bruijn are thanked for technical assistance. Dr. Theo van Walsum is thanked for assistance with image display.

REFERENCES

1. King MA, Pretorius PH, Farncombe T, Beekman FJ. Introduction to the physics of molecular imaging with radioactive tracers in small animals. *J Cell Biochem*. 2002;39(suppl):221–230.
2. Gambhir SS, Herschman HR, Cherry SR, et al. Imaging transgene expression with radionuclide imaging technologies. *Nature Neoplasia*. 2000;2:118–138.
3. Phelps ME. Inaugural article: positron emission tomography provides molecular imaging of biological processes. *Proc Natl Acad Sci USA*. 2000;97:6226–6233.
4. Weissleder R. Scaling down imaging: molecular mapping of cancer in mice. *Nature Rev Cancer*. 2002;2:11–18.
5. Rudin M, Weissleder R. Molecular imaging in drug discovery and development. *Nature Rev Drug Discov*. 2003;2:123–131.
6. Shah K, Jacobs A, Breakfield XO, Weissleder R. Molecular imaging of gene therapy for cancer. *Gene Ther*. 2004;11:1175–1187.
7. Yang Y, Tai YC, Siegel S, et al. Optimization and performance evaluation of the microPET II scanner for *in vivo* small-animal imaging. *Phys Med Biol*. 2004;49:2527–2545.
8. Jaszczak RJ, Li J, Wang H, Zalutsky MR, Coleman RE. Pinhole collimation for ultra-high-resolution small-field-of-view SPECT. *Phys Med Biol*. 1994;39:425–437.
9. Ishizu K, Mukai T, Yonekura Y, et al. Ultra-high-resolution SPECT system using four pinhole collimators for small animal studies. *J Nucl Med*. 1995;26:2282–2289.
10. Weber DA, Ivanovic M. Ultra-high-resolution imaging of small animals: implications for preclinical and research studies. *J Nucl Cardiol*. 1999;6:332–344.
11. Wu MC, Tang HR, Gao DW, et al. ECG gated pinhole SPECT in mice with millimeter resolution. *IEEE Trans Nucl Sci*. 2000;47:1218–1227.
12. Meikle SR, Fulton RR, Eberl S, Dahlbom M, Wong KP, Fulham MJ. An investigation of coded aperture imaging for small animal SPECT. *IEEE Trans Nucl Sci*. 2001;48:816–821.
13. McElroy DP, MacDonald LR, Beekman FJ, et al. Performance evaluation of A-SPECT: a high resolution desktop pinhole SPECT system for imaging small animals. *IEEE Trans Nucl Sci*. 2002;49:2139–2147.
14. Beekman FJ, Vastenhouw B. Design and simulation of a high-resolution stationary SPECT system for small animals. *Phys Med Biol*. 2004;49:4579–4592.
15. Chatziioannou A. Molecular imaging of small animals with dedicated PET tomographs. *Eur J Nucl Med Mol Imaging*. 2002;29:98–114.
16. Beekman FJ, McElroy DP, Berger F, Gambhir SS, Hoffman EJ, Cherry SR. Towards *in vivo* nuclear microscopy: I-125 imaging in mice using micro-pinholes. *Eur J Nucl Med Mol Imaging*. 2002;29:933–938.
17. Rowe RK, Aarsvold JN, Barrett HH, et al. A stationary hemispherical SPECT imager for three-dimensional brain imaging. *J Nucl Med*. 1993;34:474–480.
18. Liu Z, Kastis GA, Stevenson GD, et al. Quantitative analysis of acute myocardial infarct in rat hearts with ischemia-reperfusion using a high-resolution stationary SPECT system. *J Nucl Med*. 2002;43:933–939.
19. van der Have F, Beekman FJ. Photon penetration and scatter in micro-pinhole imaging: a Monte Carlo investigation. *Phys Med Biol*. 2004;49:1369–1386.
20. Lange K, Carson R. E.M. reconstruction algorithms for emission and transmission tomography. *J Comput Assist Tomogr*. 1984;8:306–316.
21. Metzler SD, Bowsheer JE, Smith MF, Jaszczak RJ. Analytic determination of pinhole collimator sensitivity with penetration. *IEEE Trans Med Imaging*. 2001;20:730–741.
22. Accorsi R, Metzler SD. Analytic determination of the resolution-equivalent effective diameter of a pinhole collimator. *IEEE Trans Med Imaging*. 2004;23:750–763.
23. Beekman FJ, Vastenhouw B, van der Have F. Towards 3D nuclear microscopy using locally focusing many-pinhole SPECT. In: *Proceedings of the 2003 International Meeting on Fully Three-Dimensional Image Reconstruction in Radiology and Nuclear Medicine*. Brest, France: Brest University Press; 2004:262–264.
24. Orlov SS. Theory of three-dimensional reconstruction. I. Conditions for a complete set of projections. *Sov Phys Crystallogr*. 1975;20:429–433.
25. Matherson KJ, Barber HB, Barrett HH, et al. Progress in the development of larger-area modular 64x64 CdZnTe imaging arrays for nuclear medicine. *IEEE Trans Nucl Sci*. 1998;45:354–358.
26. He Z, Li W, Knoll GF, Wehe DK, Stahle CM. 3-D position sensitive CdZnTe gamma-ray spectrometers. *Nucl Instrum Methods Phys Res A*. 1999;422:173–178.
27. Llopert X, Campbell M, Dinapoli R, Segundo DS, Pemigotti E. Medipix2: a 64-k pixel readout chip with 55- μm square elements working in single photon counting mode. *IEEE Trans Nucl Sci*. 2002;49:2279–2283.
28. Pani R, Pellegrini R, Cinti MN, et al. New devices for imaging in nuclear medicine. *Cancer Biother Radiopharm*. 2004;19:121–128.
29. de Vree GA, Westra AH, Moody I, van der Have F, Ligtvoet CM, Beekman FJ. Photon-counting gamma camera based on an electron-multiplying CCD. *IEEE Trans Nucl Sci*. In press.